Available online at www.sciencedirect.com
ScienceDirect
Scripta Materialia 61 (2009) 871–874
Scripta MATERIALIA
www.elsevier.com/locate/scriptamat

Enhanced microhardness of nanocrystalline carbon nanotube-reinforced Cu composite using planar shock-wave compaction

Ha Neul Kim,[a] Soon Nam Chang[b] and Do Kyung Kim[a,*]

[a]*Department of Materials Science and Engineering, Korea Advanced Institute of Science and Technology (KAIST), 373-1 Guseong-dong, Yuseong-gu, Daejeon 305-701, Republic of Korea*
[b]*Agency for Defense Development, Yuseong P.O. Box 35-1, Daejeon 305-600, Republic of Korea*

Received 29 May 2009; revised 10 July 2009; accepted 20 July 2009
Available online 23 July 2009

Planar shock-wave compaction (SWC), at a peak pressure of ~15 GPa, was used to fabricate 90% dense carbon nanotube-reinforced–Cu composite (SWC-CNT/Cu). Transmission electron microscopy analysis of SWC-CNT/Cu revealed retention of nanoscale size Cu grains, and the presence of shear bands and homogeneous dispersion of CNTs in the Cu matrix. These findings explain the significantly enhanced hardness observed. A Vickers hardness and nanoindentation test for SWC-CNT/Cu indicated enhanced microhardness of 1190 and 1794 MPa, respectively, proving the efficiency of the SWC technique.

Keywords: Copper; Mechanical properties; Carbon nanotube-reinforced composite; Shock-wave compaction; Microhardness

Single-step consolidation of powders using high-pressure shock-waves generated by planar impact or explosives is considered to be a potentially important method for the synthesis and processing of bulk nanocrystalline materials. The shock-wave compaction (SWC) processes occur during on microsecond timescale and involve the heterogeneous deposition of shock energy, resulting in interparticle bonding and configurational changes in particles, such as the dislocations, subgrains, distorted regions and partially melted regions [1,2]. Thus, SWC-processed dense monolithic bulks or composites are considerably different from samples densified conventionally via powder processing techniques that involve additional sintering steps at high temperature. Rapid consolidation of powders by SWC can form bulk material that retaining the nanosize of the powder without any substantial grain growth as the process is performed on such a short timescale (of the order of microseconds) that only limited heating of the particle surface regions occurs. As a result, materials processed by SWC have proved to be of considerable interest. Chen et al. [3] and Jin et al. [4] reported highly densified metal compacts with microstructural modifications, thereby improving the mechanical properties of the bulk. In addition, Akashi et al. [5], Kondo et al. [6,7], Kim et al. [8] and Komatsu et al. [9] reported on the consolidation of ceramics via SWC, which offers certain advantages over conventional processes.

In addition to the significance of the processing method to fabricate highly densified bulk nanocrystalline metals and ceramic materials, reinforcement of those matrices with carbon nanotubes (CNTs) to form composites plays a vital role in enhancing their mechanical properties. The preparation of high-quality CNT-reinforced composites involves addressing two major issues: good homogeneous dispersion of CNTs in the matrix and achieving high densification of CNT-reinforced powders to bulk.

In the present study, a planar SWC procedure was used to compact wet chemical synthesized CNT/Cu composite powder. Dynamic compaction was performed by means of 60 mm propellant-gun system that possesses certain important advantages, including planarity and parallelism at impact, which means that the process is reproducible. The SWC-CNT/Cu composite was characterized by X-ray diffraction (XRD), scanning electron microscopy (SEM) and transmission electron microscopy (TEM) techniques. The structural changes of SWC-CNT/Cu were correlated with the microhardness, measured by Vickers indentation and nanoindentation.

CNT/Cu composite nanopowder with a CNT content of ~10 vol.% was synthesized by a wet chemical oxidation–reduction process [10]. In a typical procedure,

* Corresponding author. E-mail: dkkim@kaist.ac.kr

1359-6462/$ - see front matter © 2009 Acta Materialia Inc. Published by Elsevier Ltd. All rights reserved.
doi:10.1016/j.scriptamat.2009.07.017

10 vol.% of functionalized multi-wall CNTs (Il-Jin nanotech, Korea), using a mixture of conc. HNO_3 and H_2SO_4 (1:3) [11], was homogeneously dispersed in ethanol. Copper acetate monohydrate (Aldrich) was then added to the CNT suspension, which was then sonicated for 2 h. The homogeneous suspension was dried at 80 °C for 12 h and calcined at 300 °C for 4 h. Then the powder was reduced at 250 °C for 3 h under pure H_2 atmosphere to obtain highly dispersed 10 vol.% CNT in Cu matrix. In order to confirm the effect of CNT reinforcement, pristine Cu powder was also synthesized following the above procedure without the addition of CNT.

SWC-CNT/Cu composite and SWC-Cu pellets were fabricated using a 60 mm propellant-gun system fixture. Initially, crush strength, as theoretically developed by Fischmeister and Artz [12], was measured for the synthesized CNT/Cu composite and pristine Cu powder through a static compaction method. The determined crush strength and Hugoniot data [13] (Los Alamos Shock Laboratory) were used to simulated the applied stress on the composite powder during the planar shock-wave propagation along the target fixture assemblage, using the two-dimensional AUTODYNE-2D hydrodynamic computer code. The compaction process was established by introducing a compressive stress wave into the powder capsule using an accelerated flyer plate. The P-α model, which was developed by Herrman [14] and Carrol and Holt [15,16], was applied to the target material for the description of the shock pressure and density of the CNT/Cu and pristine Cu powder response during the impact loading.

SWC on CNT/Cu composite and pristine copper powder was performed with a plate impact fixture, using the 60 mm diameter propellant-gun (Agency for Defense Development, Korea). The powder was statically pressed in a capsule to achieve ~50% packing density of the theoretical maximum density (TMD). Impact experiments were performed using a 5 mm thick steel flyer plate attached on a polycarbonate projectile accelerated in the 60 mm diameter propellant-gun, at an impact velocity of ~1000 m s^{-1}, which was measured using three in-line shorting-pins. After the shock-loading, the steel capsule was recovered and lathed carefully to remove the compacted sample. The recovered disc-shaped pellet was 12 mm in diameter and 1 mm thick.

The relative densities of the SWC-CNT/Cu and SWC-Cu pellets were measured by the Archimedes method in deionized water as an intrusion medium. The phase and crystal structure were characterized by XRD (Rigaku, D/MAX-IIIC X-ray diffractometer, Tokyo, Japan), using Cu K_α radiation ($\lambda = 0.15406$ nm at 40 kV and 45 mA). The crystallite size of the CNT/Cu and pristine Cu powders and pellets were estimated from the Scherrer equation, $D = (0.9\lambda)/(\beta \cos\theta)$, where D is the crystallite size, λ is the wavelength of incident X-rays (0.15406 nm), β is the half-width at full-maximum, and θ is the diffraction angle. The powder morphology, and the fracture and polished surface of SWC-CNT/Cu and SWC-Cu pellets, were characterized by SEM (Philips XL30 FEG, Eindhoven, the Netherlands). TEM samples were prepared by single beam focused ion beam (SB-FIB, Hitachi FB-2100, Tokyo, Japan). The grain size and selected-area electron diffraction (SAED) were characterized using a transmission electron microscope (JEOL JEM-2100F, Tokyo, Japan). The microhardness of SWC-CNT/Cu composite and SWC-Cu pellets was tested by Vickers indenter and nanoindenter (Microtest NT-2, Wrexham, UK). The nanoindentation was made in selected regions of the pellets; those regions appear to have approximately full density, which was confirmed by optical microscopy.

XRD pattern in Figure 1a shows the CNT/Cu composite powder synthesized by the wet chemical oxidation–reduction process. The pattern confirms the single phase of crystalline CNT/Cu, and is in good agreement with the JCPDS file #65-9743 of a typical face-centered cubic structure. In Figure 1a, the powders reduced at 250 °C exhibit a relatively broader peak width, which may be due to the smaller particle size. The SEM image of synthesized CNT/Cu composite powder is shown as an inset in Figure 1a; homogeneously dispersed CNTs can be seen in the matrix of Cu nanoparticles. The particle morphology indicates the aggregation of Cu particles with the individual primary particle sizes of ~50 nm. Figure 1b shows the pressure vs. density plot of the CNT/Cu composite powder. The thick line represents the performed experimental static compaction data and the thin grey line indicates the fit curve using the equation based on the Fischmeister–Artz model:

$$P_y = 2.97\rho^2\left(\frac{\rho-\rho_0}{1-\rho_0}\right)\sigma_y, \tag{1}$$

where ρ_0 is the initial packing density, σ_y is the yield strength of the powder, P_y is the applied pressure, and ρ is a certain final density. From fitted data in Figure 1c, the crush strength was determined as 201 MPa at TMD. Similarly, the crush strength was determined for the pristine Cu powder to be 280 MPa at TMD.

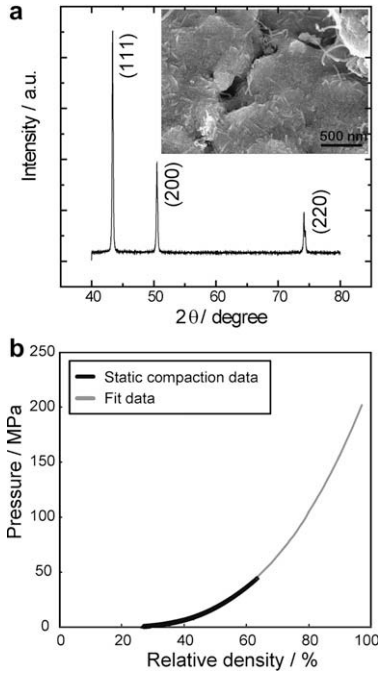

Figure 1. Synthesized CNT/Cu composite powder: (a) XRD pattern of powder (inset: SEM micrograph of powder); and (b) pressure–density curve of the powder for estimating the crush strength.

Based on the simulation result using the two-dimensional AUTODYNE-2D hydrodynamic code, the projectile velocity was set as 1000 m s^{-1}, and thus, the stress on CNT/Cu and Cu powder compact was over 15 GPa (peak pressure), which was much higher than the crush strength. As a result of the excess energy exerted by SWC on the CNT/Cu nanopowder, a few secondary effects are expected, including dislocations, subgrains, distorted regions and partially melted regions. Figure 2a shows the XRD pattern of the nanocrystalline SWC-CNT/Cu compact and the inset shows the broadened (1 1 1) peak as well as a photograph of an as-recovered pellet after SWC. The pattern confirms the composite is single-phase nanocrystalline CNT/Cu even after shock compaction, and is in good agreement with the powder pattern shown in Figure 1a. The crystallite size is estimated using the Scherrer equation considering the broadened (1 1 1), (2 0 0) and (2 2 0) peaks in Figure 2a; and the crystallite sizes are ~43 nm for SWC-Cu, and ~79 nm for SWC-CNT/Cu. Figure 2b shows the SEM micrograph of a Vickers indented surface of a SWC-CNT/Cu pellet. It is evident from Figure 2b that a few of pores exist, indicating complete densification was not achieved under the estimated consolidation condition, i.e. relative green density of 50% and peak pressure of 15 GPa. The insets in Figure 2b show SEM images of the polished (right) and fracture (left) surfaces of the cross-sectional view of a SWC-CNT/Cu pellet. The polished surface image reveals homogeneous dispersion of CNTs with nanosize Cu grain. The fracture surface reveals homogeneous dispersion of CNTs embedded with the nanoparticles of Cu matrix and CNT pull-out, which confirms the high-quality reinforcement of the CNT/Cu composite. Thus, homogeneously dispersed, CNT-reinforced Cu composite pellet fabricated via planar SWC is expected to exhibit enhanced mechanical properties. The estimated relative densities via the Archimedes method for SWC-Cu and SWC-CNT/Cu pellets are ~90% TMD. Figure 1a and b in the Supplementary material shows SEM images of a Vickers indentation and the fracture surfaces of a SWC-Cu pellet. It is evident from these SEM images that a few of pores exist comparable with the 90% TMD under the estimated consolidation condition, i.e. initial relative density of 50% and peak pressure of 15 GPa. Furthermore, the fracture surface of the SWC-Cu pellet consists of nanosize grains, which is consistent with the crystallite size estimated from the Scherrer equation.

TEM images of the SWC-CNT/Cu composite pellets are shown in Figure 3a and b. The images reveal that the matrix consists of Cu nanograins ranging from 50 to 100 nm. The presence of nanograins in Figure 3a and b indicates the retention of the powder Cu particle size, which evidently confirms the suppression of grain growth during the planar SWC process. Figure 3c shows the presence of subgrains with neat grain boundaries of different orientations as represented by grains A and B and their corresponding SAED images, which is attributed to the (1 1 1) plane. Figure 3d shows the presence of a shear band that formed during the peak pressure shock compact and contains a number of grains 100 nm thick and 300 nm long. The formation of shear bands may be due to the combined effect of thermal energy generated during the shear localization of high-amplitude compressive stress and combination of particles. The high-resolution TEM images presented in Figure 3e and f show the moiré fringes due to the overlapping of grains caused by SWC. In addition, the

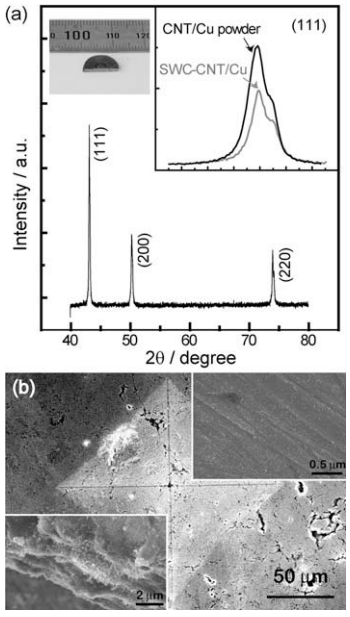

Figure 2. SWC-CNT/Cu composite: (a) XRD pattern of shock compact, showing a comparison of the XRD patterns of CNT/Cu powder and SWC-Cu compact; and (b) Vickers indented surface containing pores and microcracks (right inset: cross-section of a shock compact in which CNTs (white spots) were embedded; left inset: the fracture surface of a shock compact where CNT pull-out occurred).

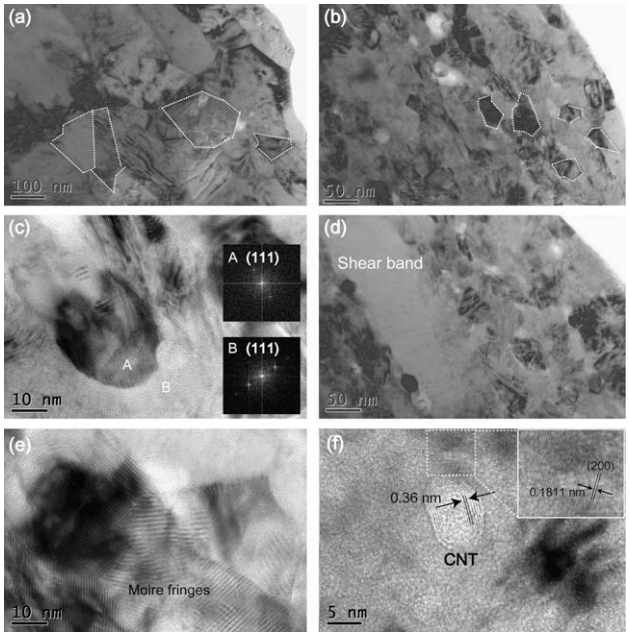

Figure 3. TEM micrographs of SWC-CNT/Cu composite: (a) grain size of Cu matrix is ~100 nm; (b) grain size of Cu matrix is ~50 nm; (c) the presence of nano- and subgrains with neat grain boundaries of different orientations as represented by grainsA and B; (d) the presence of shear bands formed with particles 100 nm thick and 300 nm long; (e) moiré fringes due to the overlap of grains; and (f) the dispersed CNTs in the Cu matrix and the clear lattice fringes of the compacted Cu.

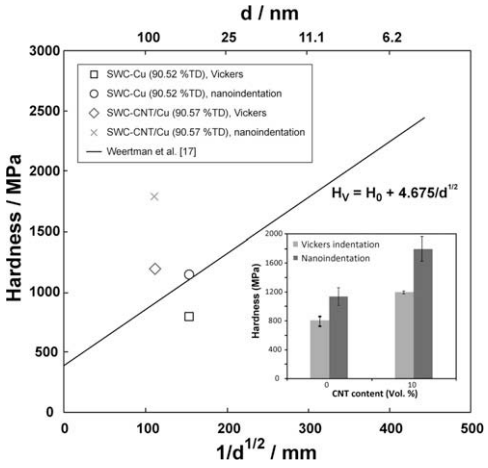

Figure 4. The hardness values for the SWC-Cu and SWC-CNT/Cu composites plotted as a function of grain size of the Cu matrix and compared with the values reported by Weertman et al. based on the Hall–Petch relationship of pure polycrystalline Cu [17].

dispersal of CNTs in the Cu matrix is confirmed by the wall thickness of 0.36 nm. The inset image in Figure 3f shows the clear lattice fringes of the compacted Cu grains measuring 0.181 nm, which indicates the d-spacing of the (2 0 0) plane.

The Vickers indentation and nanoindentation tests were conducted for the SWC-Cu and SWC-CNT/Cu pellets under 12 N loads for 15 s and under 50 mN loads for 10 s, respectively. The Vickers hardnesses of SWC-Cu and SWC-CNT/Cu composite pellets are 803 and 1190 MPa, respectively, and the hardness values based on nanoindentation are 1134 and 1794 MPa, respectively. Figure 4 shows the hardness values for the SWC-Cu and SWC-CNT/Cu composites plotted as a function of grain size of Cu matrix and compared with the values reported by Weertman et al. using the Hall–Petch relationship for pure polycrystalline Cu [17]. The measured Vickers hardness of SWC-Cu with grain size ~43 nm exhibits a lower hardness than the value expected based on the Hall–Petch relationship. This may be due to the presence of 10% porosity in the sample. On the other hand, the SWC-CNT/Cu composite with grain size ~79 nm had a higher hardness value than predicted from the Hall–Petch relationship even though the pellets contains 10% porosity. The higher microhardness of SWC-CNT/Cu composite can attribute to the combined effect of SWC technique and reinforcement of CNTs in the Cu matrix.

The planar SWC procedure was successfully used with a peak pressure of 15 GPa and fabricated 90% dense SWC-CNT/Cu composite. The microstructure of the shock-consolidated compacts exhibited homogeneous dispersion of CNTs in the Cu matrix, including nano- and subgrains, distorted regions, and shear bands caused by shock-loading. The Vickers indentation and nanoindentation confirmed that the SWC-CNT/Cu composite pellets exhibited an enhanced microhardness. The reinforcement of CNTs in the Cu matrix combined with the efficient SWC technique yielded a matrix of nano- and subgrains size, and resulted in enhanced microhardness.

This work was financially supported by Defense Acquisition Program Administration and Agency for Defense Development under the contract UD060006AD and the Korea Research Foundation Grant funded by the Korean Government (MOEHRD) (KRF-2005-005-J09701).

Supplementary data associated with this article can be found, in the online version, at doi:10.1016/j.scriptamat.2009.07.017.

[1] M.A. Meyers, Dynamic Behavior of Materials, John Wiley, New York, 1994.
[2] V.F. Nesterenko, Dynamics of Heterogeneous Materials, Springer-Verlag, New York, 2001.
[3] T. Chen, J.M. Hampikian, N.N. Thadhani, Acta Mater. 47 (1999) 2567.
[4] Z.Q. Jin, K.H. Chen, J. Li, H. Zeng, S.F. Cheng, J.P. Liu, Z.L. Wang, N.N. Thadhani, Acta Mater. 52 (2004) 2147.
[5] T. Akashi, A. Sawaoka, J. Am. Ceram. Soc. 69 (1986) C–78.
[6] K. Kondo, S. Soga, E. Rapoport, A. Sawaoka, M. Araki, J. Mat. Sci. 21 (1986) 1579.
[7] K. Kondo, S. Soga, A. Sawaoka, M. Araki, J. Mat. Sci. 20 (1985) 1033.
[8] H.N. Kim, S.N. Chang, D.K. Kim, Int. J. Mod. Phys. B 22 (2008) 1686.
[9] T. Komatsu, Phys. Chem. Chem. Phys. 6 (2004) 878.
[10] K.T. Kim, S.I. Cha, S.H. Hong, Mat. Sci. Eng. A Struct. 430 (2006) 27.
[11] S.F. McKay, J. Appl. Phys. 35 (1964) 1992.
[12] H.F. Fischmeister, E. Arzt, Powder Metall. 26 (1983) 82.
[13] S.P. Marsh, LASL Shock Hugoniot data, University of California Press, Los Alamos, 1980.
[14] W. Herrmann, J. Appl. Phys. 40 (1969) 2490.
[15] M. Carroll, A.C. Holt, J. Appl. Phys. 43 (1972) 759.
[16] M. Carroll, A.C. Holt, J. Appl. Phys. 43 (1972) 1626.
[17] J.R. Weertman, Mat. Sci. Eng. A Struct. 166 (1993) 161.